Irradiation-driven amorphous-to-glassy transition in quartz: The crucial role of the medium-range order in crystallization

N. M. Anoop Krishnan,[1] Bu Wang,[1,2] Yann Le Pape,[3] Gaurav Sant,[2,4] and Mathieu Bauchy[1]

[1]*Physics of AmoRphous and Inorganic Solids Laboratory (PARISlab), Department of Civil and Environmental Engineering, University of California, Los Angeles, California 90095, USA*

[2]*Laboratory for the Chemistry of Construction Materials (LC2), Department of Civil and Environmental Engineering, University of California, Los Angeles, California 90095, USA*

[3]*Oak Ridge National Laboratory, P.O. Box 2008, Oak Ridge, Tennessee 37831-6148, USA*

[4]*California Nanosystems Institute (CNSI), University of California, Los Angeles, California 90095, USA*

(Received 7 April 2017; revised manuscript received 3 October 2017; published 26 October 2017)

Noncrystalline solids can be classified into glassy and amorphous, wherein glasses and amorphous solids relax toward the supercooled liquid and crystalline states upon heating, respectively. However, the structural origin of such distinction remains unknown. Herein, based on molecular-dynamics simulations of irradiation-induced disordering of α-quartz, we demonstrate the existence of an amorphous-to-glassy transition. We show that the transition to the glassy state originates from the appearance of structural defects within the medium-range order of the atomic network. Such defects arise from the percolation of short-range defects and kinetically prevent crystallization. Overall, this suggests that the propensity of a disordered system for crystallization is controlled by the similarity between its medium-range order and that of the isochemical crystal.

DOI: 10.1103/PhysRevMaterials.1.053405

I. INTRODUCTION

When cooled from the liquid state, materials can turn into solids by crystallizing, wherein crystals exhibit a periodic atomic structure. In contrast, if quenched fast enough to avoid crystallization, solids can also be noncrystalline, that is, they can feature a disordered atomic network [1]. Noncrystalline solids typically show a rather well defined short-range order (SRO, comprising bond lengths, bond angles, and coordination numbers) and some degree of medium-range order (MRO, comprising dihedral angles, ring statistics, etc.). However, in contrast to crystals, they lack any long-range order (LRO, i.e., structural correlations larger than around 10 Å) [1]. Disordered materials can also be formed through various techniques, including sol-gel synthesis, vapor deposition, or exposure to shock waves or radiations [1–3].

Although the terms "glasses" or "amorphous" are commonly used interchangeably to describe noncrystalline solids, we rely here on the classification introduced by Gupta [1,4,5], wherein "amorphous" and "glassy" refer to two mutually exclusive states for disordered solids, as defined in the following. First, based on their SRO, glasses satisfy the condition SRO(glass) = SRO(melt), whereas amorphous solids (a-solids) violate this condition, i.e., SRO(a-solid) ≠ SRO(melt). Second, when exposed to higher temperatures, amorphous solids do not show any relaxation toward the liquid state, and, consequently, they do not exhibit a glass transition. Instead, upon heating, they tend to relax toward the crystalline state [4]. Based on this observation, a more meaningful classification of disordered solids has been proposed [3,5], wherein *glasses* are defined as "*a nonequilibrium, noncrystalline state of matter that appears solid on a short time scale but continuously relaxes towards the liquid state*." In turn, noncrystalline solids that tend to crystallize upon heating are referred to as *amorphous* [4]. In other words, although glasses and amorphous solids are both out-of-equilibrium materials, glasses tend to relax toward the metastable supercooled liquid state upon heating (e.g., glassy silica, g-SiO_2), whereas amorphous solids tend to relax toward the stable crystalline state [4] (e.g., amorphous silicon, a-Si [6]). Altogether, the criterion proposed by Gupta offers a physically sound framework to distinguish amorphous from glassy solids. As such, note that, in the following, we establish our conclusions by entirely relying on this framework. However, despite the convenience of this criterion, no clear structural signature discriminating glassy from amorphous atomic networks has been established thus far.

Here, based on reactive molecular dynamics (RMD) simulations, we report evidence of an *amorphous-to-glassy* (ATG) transition, and we identify its underlying structural origin. This is illustrated by taking the example of α-quartz, wherein the degree of disorder is progressively increased through irradiation. We observe that, at low deposited irradiation energy, the system recrystallizes upon heating and eventually shows a first-order transition to the liquid state. In contrast, it continuously converts into a liquid at higher deposited energy, thereby fulfilling the definition of a glass. We show that this transition is associated with the appearance of MRO defects in the atomic network. We demonstrate that the ATG transition arises from the fact that, upon thermal annealing, SRO defects can be "*healed*," whereas MRO defects cannot. This suggests that the structural similarity between the MRO of disordered atomic networks and their crystalline counterparts plays a crucial role in controlling their propensity for crystallization.

II. SIMULATION METHODS

A. Irradiation simulations

Following a well-established methodology [2,7–9], we rely here on realistic RMD simulations of irradiation-induced damage in α-quartz. All the simulations are conducted using the open-source package LAMMPS [10]. To simulate the irradiation of the network by neutrons, a randomly chosen atom is accelerated with a kinetic energy (600 eV herein)

that simulates an elastic collision of the neutron particle with the primary knock-on atom (PKA). Since the probability of neutron collision differs for each of the atomic species, the PKA is chosen based on weighted probabilities accounting for the neutron cross sections of silicon and oxygen atoms. The PKA, accelerated with the desired incident energy, then collides with other atoms in the lattice, thereby resulting in a ballistic cascade. To avoid any spurious effects of the thermostat on the dynamics of the cascade, a spherical region is created around the impacted zone. The atoms outside the spherical region are kept at a constant temperature of 300 K by a Nosé-Hoover thermostat [11], while the atoms inside the sphere are treated in the *NVE* ensemble. Note that high velocities and excessive collisions during the damage cascade could result in numerical errors within the time integration. To avoid such errors, a variable time step is used during the ballistic cascade, which is based on the maximum distance moved by the PKA during one time step. Otherwise, a constant time step of 0.5 fs is used. Based on the time required herein for the temperature and energy of the system to converge after each collision, the relaxation of the ballistic cascade is simulated for 15 ps. The system is further relaxed in the *NPT* ensemble at 300 K and zero pressure for another 5 ps. This enables the system to adjust its density upon irradiation. Thus, a simulation time of 20 ps is used per PKA to ensure the full relaxation of the system under irradiation. The process is then repeated with different atomic species as PKA until the system exhibits both long-range and short-range saturation, i.e., in terms of both enthalpy and density. It is worth noting that the sequential irradiation methodology presented here yields similar cumulative damage to that of simultaneous multiple particle irradiation [12]. This ensures that the generality of the results is maintained.

Due to the high velocity and displacement of the PKA, a large region within the crystal lattice is affected during each ballistic cascade. Consequently, to avoid potential spurious self-interactions arising from the periodic boundary conditions, an appropriate minimum system size needs to be determined for a given deposited energy per PKA. However, extremely large system sizes might be computationally prohibitive. Herein, we employ the following methodology to determine the optimum system size. First, each of the atomic species present in the pristine quartz (Si and O atoms) is repeatedly projected with the target radiation energy in randomly chosen directions. Then, the maximum atomic displacements of each of the PKAs are recorded. Finally, the system size is chosen to be at least twice as large as the maximum distance among all the recorded ones. In the present case, the optimal initial system size is obtained as a $10 \times 10 \times 9$ α-quartz supercell comprising 8100 atoms. Note that the present size obtained based on such optimization is significantly smaller than previous studies wherein an arbitrarily large system size was chosen. It is worth noting that the accuracy of molecular-dynamics simulations depends highly on the ability of interatomic potentials to appropriately describe the structure and dynamics of the system. In the case of irradiation simulations, this is further complicated by the fact that the system undergoes a structural disordering. In particular, the interatomic potential must (i) be able to describe both the pristine and disordered structures with a fixed set of parameters; (ii) provide a realistic description of ballistic cascades resulting from high-energy collisions, that is, wherein atoms potentially explore the short-distance part of the potential; and (iii) be able to handle the formation of local structural defects—e.g., over- or undercoordinated atoms—which are likely to form upon irradiation. Toward that end, we use the ReaxFF potential [13], with parameter calibrations from Manzano *et al.* [14], as it can correctly describe the structure of both pristine α-quartz and glassy silica, and it features robust potential forms that can dynamically adjust the potential energy based on the local atomic environment of each atom [15].

B. Computation of the fraction of displaced atoms

To determine at which point the system becomes fully disordered—that is, when no pristine regions remain in the system—we compute the fraction of impacted atoms upon irradiation. This is achieved by computing the fraction of permanently displaced atoms after each bullet impact. Note that the displacements are computed after the complete relaxation of the system after each ballistic cascade. Further, the movement of the center of mass of the system, if any, is removed from the displacements in order to get the actual displacement of the atoms with respect to their lattice position at equilibrium. Note that, based on the Lindemann criterion for phase transition [16], melting initiates in a solid when the average amplitude of the thermal vibration of a bond exceeds 10% of its original value. Here, an atom is considered displaced if it moves from its lattice position by more than 0.32 Å—20% of the of Si–O bond length—which is twice as large as the threshold proposed by the Lindemann criterion.

C. Glass preparation

To compare the response of irradiated quartz upon annealing to that of its glassy counterpart, a silica glass is prepared following the conventional melting-quenching method [15]. Note that, for a meaningful comparison with irradiated quartz, we ensure the usage of the same potential, time step, and system size (8100 atoms). First, an initial system is generated by randomly placing Si and O atoms in a cubic box while maintaining charge neutrality and ensuring the absence of any unrealistic overlap. The system is then melted at 4500 K under zero pressure for 1 ns in the *NPT* ensemble to ensure the loss of the memory of its initial configuration and to reach the state of an equilibrium silica melt. The melt is then gradually cooled from 4500 to 300 K at zero pressure with a cooling rate of 1 K/ps in the *NPT* ensemble. The final glass structure formed is further equilibrated at 300 K and zero pressure for 1 ns in the *NPT* ensemble to ensure the complete relaxation of the structure. Note that, although the cooling rate used herein for the preparation of the glass is significantly higher than that typically achieved experimentally, it has been shown that the structure of simulated silica glass depends only weakly on the cooling rate [17,18] and shows good agreement with experimental data [15].

D. Computation of the ground-state enthalpy

In this study, we aim to track the enthalpy of irradiated quartz at different annealing temperatures. This enables a

direct comparison of the energy state of partially irradiated quartz samples with those of pristine quartz and glassy silica. Further, it can be used to assess the extent of structural relaxation in irradiated quartz upon annealing. However, at finite temperature, the energy of a system comprises some contributions from the random thermal vibrations of the atoms. Such fluctuations contribute to some uncertainty in the instantaneous potential energy of the system when sampled randomly from the configurational space. This issue is overcome by computing the ground-state enthalpy H_0, which removes the random thermal fluctuations and calculates the enthalpy of the inherent structure. Thus, H_0 corresponds to the energy of a configurational state at 0 K. This is computed by performing an energy minimization at zero pressure, following the method presented in Ref. [19]. This ensures that all atoms reach a local minimum of potential energy, thereby removing any thermal contribution from the computed enthalpy. Note that this method provides the local—i.e., not absolute—minimum of enthalpy of the system, and, as such, it can be used to obtain the value of the ground-state enthalpy at a given temperature. Such evolutions are investigated for α-quartz, glassy silica, and quartz samples subjected to different radiation dosage using the following procedure. Starting from structures equilibrated at 300 K and zero pressure, the system is gradually heated at a rate of 1 K/ps under zero pressure in the *NPT* ensemble up to a temperature of 4500 K, that is, when both the crystal and glass melt. *A posteriori*, independent atomic configurations are selected every 100 K, instantaneously cooled to 1 K, and further relaxed for 50 ps at this temperature in the *NPT* ensemble. The ground-state enthalpy is eventually computed for each configuration.

E. Computation of the enthalpy of fusion

To characterize the solid-to-liquid phase transformation of irradiated quartz samples—and thereby discriminate glassy from amorphous systems—we compute their enthalpy of fusion, ΔH_f, that is, the extent of the enthalpy discontinuity upon melting. ΔH_f is calculated through the following methodology. First, the ground-state enthalpy, H_0, is plotted as a function of the annealing temperature. The derivative of H_0 with respect to the temperature is then computed numerically to obtain the instantaneous slope of the H_0 versus T curve. This derivative, dH_0/dT, is then plotted as a function of the annealing temperature. At the melting temperature, the discontinuity in H_0 results in a peak in the dH_0/dT curve. ΔH_f is then obtained by computing the area under this peak in the dH_0/dT curve around the melting temperature. Note that a baseline is fitted for the dH_0/dT curve to avoid any spurious effects of the thermostat and energy-minimization techniques on the computation of ΔH_f. ΔH_f is computed for all the irradiated configurations, pristine quartz, and glassy silica following this procedure.

F. Bond-orientational parameter

The bond-orientational parameter [20] (BOP), q_l, which characterizes the local orientational order in an atomic system, is defined as

$$q_l = \sqrt{\frac{4\pi}{2l+1}\sum_{m=-l}^{m=l} \bar{Y}_{lm}\bar{Y}^*_{lm}}, \tag{1}$$

where $\bar{Y}_{lm} = \frac{1}{nnn}\sum_{j=1}^{nnn} Y_{lm}(\theta(r_{ij}),\phi(r_{ij}))$ are defined in terms of spherical harmonics Y_{lm}, and $\theta(r_{ij})$ and $\phi(r_{ij})$ are the angles corresponding to the position vector r_{ij} of the neighbor atom j with respect to the central atom i. The value $l = 3$ is then used to calculate the tetrahedral BOP q_3 [21], which is the first nonzero value for Si atoms in pristine quartz. Note that the q_3 of Si atoms with coordination numbers other than 4 is zero by definition. As such, the average q_3 captures the effects of miscoordination and internal straining in Si tetrahedra.

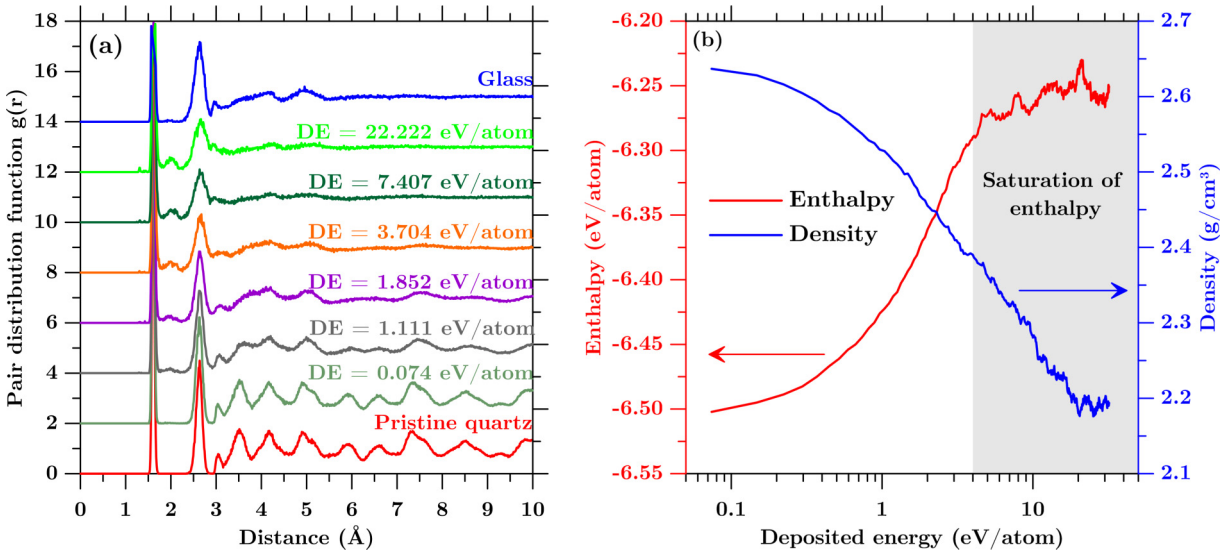

FIG. 1. (a) Pair distribution functions of pristine α-quartz, irradiated quartz with increasing dosages of deposited energy (DE), and glassy silica. (b) Enthalpy and density of quartz as a function of the deposited energy under irradiation. The gray area indicates the range of deposited energies after which enthalpy saturates, which corresponds to the glassy domain (see Fig. 4).

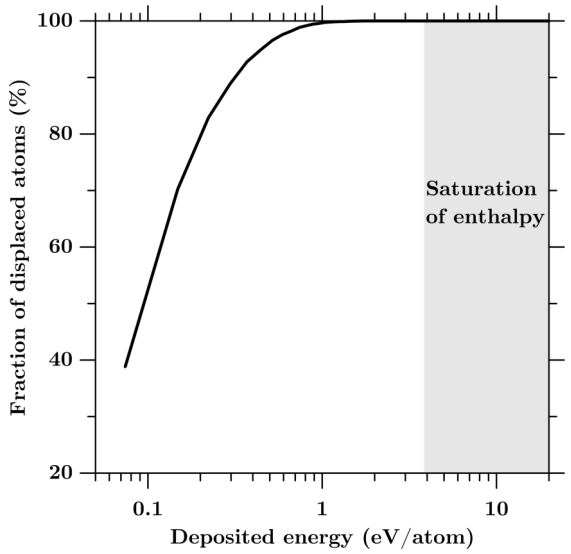

FIG. 2. Fraction of displaced atoms with respect to deposited energy in quartz. The gray area indicates the range of deposited energies after which enthalpy saturates, which corresponds to the glassy domain (see Fig. 4).

III. RESULTS

Irradiation results in a gradual disordering of the quartz network, which can be observed from the pair distribution function (PDF), as shown in Fig. 1(a). Overall, starting from the PDF of pristine quartz, we observe (i) a broadening of the SRO peaks, which denotes an increase of disorder in the short range; (ii) the appearance of an extra peak around 2 Å, arising from miscoordinated Si atoms [22]; and (iii) the disappearance of the peaks at a distance larger than 6 Å, which originates from a loss of LRO. As shown in Fig. 1(b), the formation and accumulation of energetically unfavorable defects result in an increase in the enthalpy of quartz, whereas density is found to decrease down to a value close to that of glassy silica [23] ($\rho \approx 2.20$ g/cm^3). Interestingly, we observe that the saturation of the enthalpy occurs at a lower deposited energy than that of the density. This decoupling of the enthalpy and density suggests that these properties are controlled by distinct structural features. Note that a detailed study of the structure of irradiated quartz and experimental validations can be found in Refs. [7,22,24].

Note that, at very low deposited energies, the system is only partially irradiated and exhibits both pristine and disordered regions. However, due to the limited size of the simulated system, only a few neutrons are needed to fully impact the whole atomic network. To identify the deposited energy at which the system is completely disordered, we compute the fraction of displaced atoms in quartz (see Sec. II). Figure 2 shows the fraction of displaced atoms in quartz with respect to the deposited energy. We observe that each neutron affects a notable percentage of atoms. Approximately 3200 atoms are permanently displaced by each neutron bullet on average. Further, we observe that almost all the atoms of the system are displaced at a deposited energy of 1 eV/at. This value is much lower than the deposited energy at which the saturation of enthalpy occurs (see Fig. 1).

We now investigate whether these disordered structures are glassy or amorphous, that is, whether they relax toward the crystalline or supercooled liquid state upon thermal annealing. Toward that end, six irradiated quartz samples are selected, with values of deposited energy belonging to various domains: (i) before saturation of the enthalpy; (ii) after saturation of the enthalpy, but before that of the density; and (iii) after saturation of the both the enthalpy and density. These configurations are then gradually heated (see Sec. II), and their behavior is compared to those of pristine quartz and glassy silica (as prepared by quenching a liquid; see Sec. II). Figures 3(a) and 3(b) show the ground-state enthalpy (H_0) and density (ρ), respectively, of the considered systems upon annealing.

First, we focus on the response of pristine quartz and glassy silica to heating. We observe that the H_0 of glassy silica is fairly comparable to that of pristine quartz at 300 K [see Fig. 3(a)], in accordance with Zachariasen's prediction, that is, that a glass should possess an energy comparable to that of a crystal to avoid a strong driving force for crystallization [25]. Further,

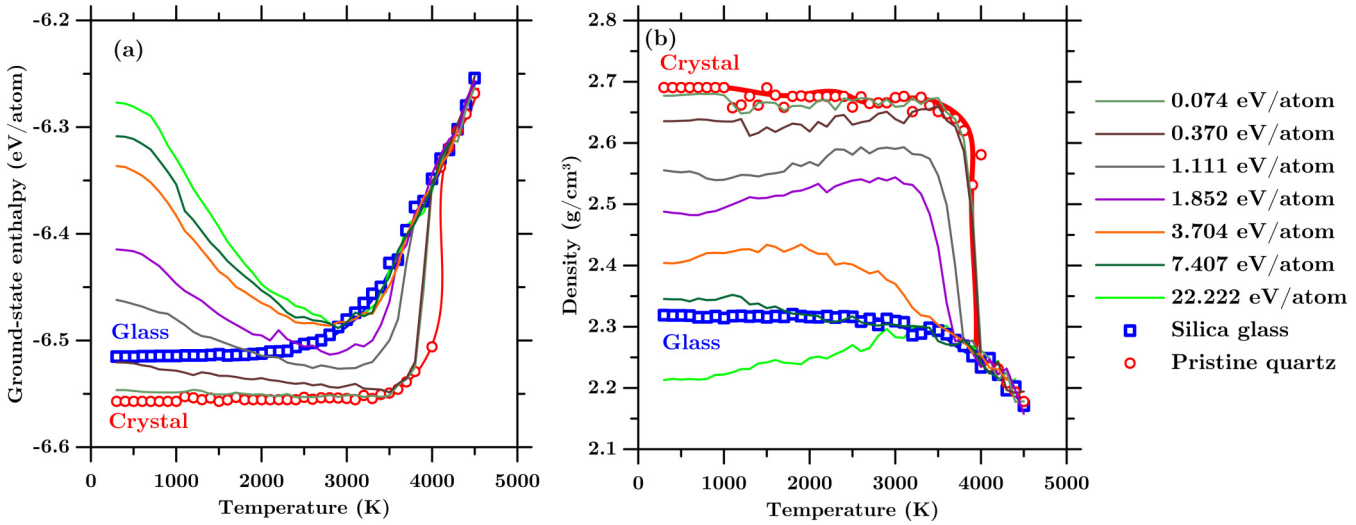

FIG. 3. (a) Ground-state enthalpy, H_0, and (b) density, ρ, as a function of the annealing temperature for α-quartz under increasing dosages of deposited energy under irradiation. The ground-state enthalpy of glassy silica is plotted for reference.

we note that the crystal does not exhibit any significant change in H_0 or ρ upon heating, until its melting point. At this point, we observe a sudden jump in both H_0 and ρ, which denotes a first-order crystal-to-liquid phase transition. On the other hand, at low temperature, glassy silica also shows little changes in its enthalpy and density. However, in contrast with crystalline quartz, further heating results in a continuous decrease in ρ and an increase in H_0. At this point, both the H_0 and ρ of glassy silica become aligned with those of the equilibrium liquid (obtained by melting crystalline quartz), which indicates a glass-to-supercooled-liquid transition. As expected, this transition is not associated with any discontinuities in H_0 or ρ.

Next, we focus on the thermal response of the irradiated configurations at low deposited energy (<3.5 eV/at). Upon heating, we observe that the system relaxes toward the pristine quartz structure [see Figs. 3(a) and 3(b)], which manifests by an initial decrease in H_0 and an increase in ρ. Note that, in the case of the configurations with deposited energies of 1.111 and 1.852 eV/at, H_0 does not fully relax to that of the crystalline state, which can arise from the limited relaxation time available for the system herein. However, in both cases, H_0 reaches values that are lower than that of the silica glass upon heating, which clearly indicates a propensity for crystallization. Further heating then results in a first-order phase transition, similar to that observed during the melting of the pristine quartz crystal. Overall, this indicates that, at low deposited energy, the disordered configurations are notably different from defective crystals, and they can be called amorphous.

Finally, we now focus on the thermal response of the irradiated configurations at high deposited energy (>3.5 eV/at). We observe that, as in the case of the configurations with low deposited energies, the values of H_0 and ρ initially decrease and increase, respectively. However, in this case, all systems are found to relax toward the glassy or supercooled liquid state [see Figs. 3(a) and 3(b)]. In particular, in contrast with the configurations with low deposited energies, H_0 does not become lower than that of the silica glass. In addition, no discontinuity in H_0 and ρ is observed at larger temperature, indicating the absence of any first-order transition. This demonstrates that, at high deposited energy, the disordered configurations are glassy.

Overall, these results show that, upon irradiation, quartz undergoes an amorphous-to-glassy transition [26–30]. Such a transition is clearly different from a traditional phase transition—such as melting—since the two participating states cannot be qualified as being some phases in the traditional thermodynamic sense. Nevertheless, in analogy with the glass transition—which occurs between a metastable supercooled liquid and a nonequilibrium glassy state—the amorphous-to-glassy transition observed here occurs between two distinct, well-defined nonequilibrium states. Note that the present results are in line with experimental studies performed by Primak *et al.* [31], wherein the density of quartz samples subjected to low irradiation dosages (early stage) was found to increase toward that of the crystal, whereas that of samples subjected to high irradiation dosages (final stage) was found to increase toward that of the glass.

To meaningfully discriminate amorphous from glassy samples, we compute the enthalpy of fusion (ΔH_f), which corresponds to the discontinuity of enthalpy upon the first-order crystal-to-liquid phase transition (see Sec. II). Note that, in contrast to crystals, glasses do not feature any enthalpy of fusion since they continuously transform to the supercooled liquid state. Figure 4 shows the evolution of ΔH_f as a function of the deposited energy. We observe that, at low deposited energy, ΔH_f has a nonzero value, which denotes the existence of a first-order crystal-to-liquid phase transition. In contrast, for values of deposited energy larger than around 4 eV/at, ΔH_f drops to zero, which indicates the absence of any underlying first-order phase transition. This allows us to locate the position of the amorphous-to-glassy transition (4 eV/at) and, as such, to clearly discriminate amorphous from glassy systems. These results the constitute evidence of an amorphous-to-glassy transition driven by gradual disordering.

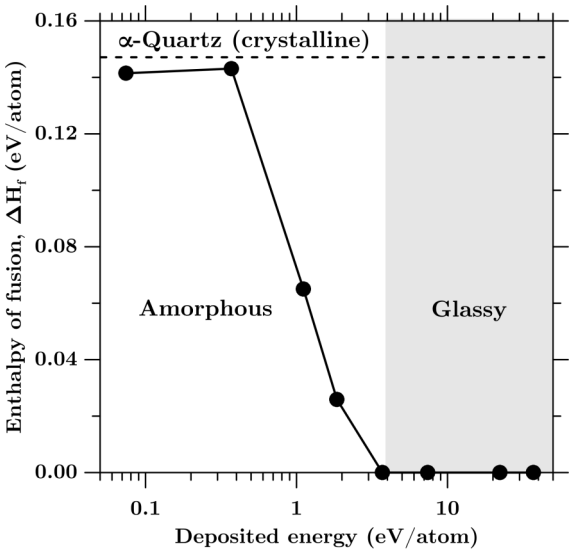

FIG. 4. Enthalpy of fusion of irradiated quartz samples with respect to the deposited energy. The white and gray areas indicate the extents of amorphous and glassy domains, respectively.

We now investigate the structural origin of the amorphous-to-glassy transition evidenced herein. First, as shown in Fig. 1(a), we note that the pair distribution does not highlight any significant structural evolutions around the location of the amorphous-to-glassy transition. However, interestingly, we observe that the location of the amorphous-to-glassy transition coincides with the saturation of the enthalpy upon irradiation [see Fig. 1(b)], whereas the density continues to decrease at this point. As such, since enthalpy depends mostly on the short-range interactions among atoms, whereas density is a more complex property that also depends significantly on the MRO, the decoupling of these properties suggests that the amorphous-to-glassy transition might be governed by the balance among the SRO and MRO defects in the network.

To investigate the role of disorder at different spatial scales in controlling the propensity for crystallization upon heating, we independently characterize the extent of structural disorder in the SRO and MRO. Since the SRO mostly arises from Si–O correlations in quartz and silica, we first compute for Si atoms the average tetrahedral bond-orientational parameter [20] (q_3; see Sec. II), which characterizes local distortions inside the SiO_4 tetrahedra. In turn, longer-range correlations can be characterized by computing the structure factor. In particular,

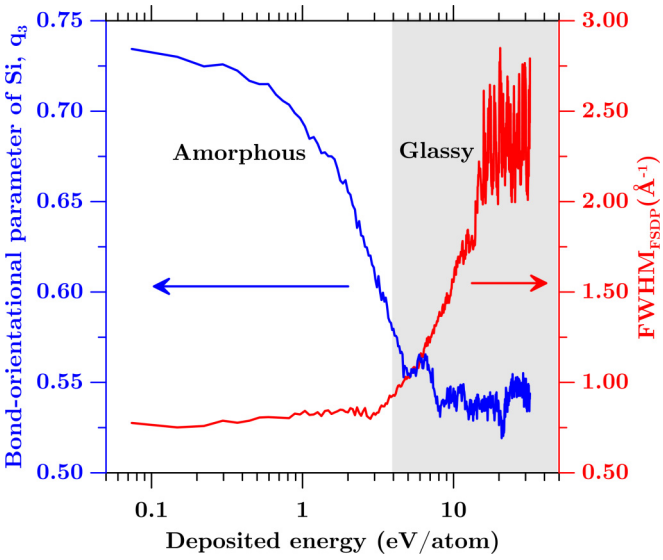

FIG. 5. Tetrahedral bond-orientational parameter (q_3) of the Si atoms and full width at half-maximum (FWHM) of the first sharp diffraction peak (FSDP) as a function of the deposited energy in α-quartz under irradiation. The white and gray areas indicate the extent of the amorphous and glassy domains, respectively (see Fig. 4).

the first sharp diffraction peak (FSDP) of the structure factor captures the extent of structural ordering at intermediate length scales in glasses [32–34]. While the origin of the FSDP remains controversial, it has been suggested to arise from the existence of structural correlations of atomic clusters or voids in the MRO [33,34]. In addition, the full width at half-maximum (FWHM) of the FSDP is inversely linked to a coherence length L in the MRO, following $L = 7.7/\mathrm{FWHM}$ [33]. In polycrystals, the coherence length is linked to the average size of the microcrystals, following the Scherrer equation [35]. Although the interpretation of the coherence length in disordered networks remains less clear, it has been suggested to be linked to the average size of rigid clusters within the atomic network [33]. As such, we compute this quantity to characterize the spatial extent of the medium-range structural correlations upon irradiation.

Figure 5 shows the evolution of q_3 and the FWHM of the FSDP as a function of the deposited energy in irradiated quartz. We observe that q_3 decreases upon irradiation, in agreement with the fact that more and more defects accumulate in the SRO through the formation of over- and undercoordinated Si atoms along with the distortion of Si tetrahedra. Note that q_3 appears strongly correlated to the enthalpy, which confirms *a posteriori* that the enthalpy depends mostly on the SRO. In contrast, the FWHM of the FSDP increases, which corresponds to a decrease of the coherence length and, thereby, to a loss of order at intermediate length scales. At saturation, the coherence length eventually reaches a value of around 3.2 Å, which is close to the typical size of the SiO_4 tetrahedra. This indicates that, eventually, structural correlations are limited to the intra-tetrahedron order.

Interestingly, we observe a clear transition within the types of defects that are formed upon irradiation. Namely, at low deposited energy, the deposited energy results in the creation of SRO defects, while the MRO remains largely unaffected, that is, the FWHM of the FSDP remains constant. However, as q_3 reaches a critical value of around 0.6, the FWHM of the FSDP suddenly starts to increase, whereas, at this point, q_3 shows a plateau. This shows that, after this critical threshold, the deposited energy tends to impact the MRO, while the SRO remains unaffected. This transition can be explained as follows. At low deposited energy, the network remains close to that of a crystal, with little internal flexibility, if any. As such, the SRO defects that are formed cannot be relaxed by the network and tend to accumulate. In turn, the accumulation of SRO defects enhances the flexibility of the network. At a critical threshold, SRO defects percolate through the system. This renders the system macroscopically flexible, so that the MRO starts to be affected by any additional deposited energy. At this point, the system gains a "*self-healing*" behavior, that is, it becomes able to locally deform to relax the formation of any additional energetically unfavorable SRO defects. This proposed mechanism is consistent with the fact that quartz shows a rigid-to-flexible transition upon irradiation [24] and eventually reaches the enthalpy landscape of a liquid, that is, with low-energy barriers, which facilitates structural relaxations within the network [36].

To establish the proposed mechanism, we characterize the size of SRO defect clusters (referred to as defect clusters hereafter) within the atomic network. First, we discriminate intact from defective Si tetrahedra by computing their respective q_3, wherein a tetrahedron is considered defective if $q_3 < 0.7$. Note that this value was chosen arbitrarily as it lies between the ranges of q_3 values associated with pristine Si tetrahedra in quartz and those associated with obviously defective Si units (i.e., for under- or overcoordinated species). However, small variations in the choice of this threshold did not significantly affect the fraction of defective Si units, which is due to the fact that defective units mostly comprise miscoordinated Si atoms, for which q_3 is zero. A defect cluster is then defined as a group of defective Si atoms mutually connected by at least one bridging oxygen atom. Finally, the spatial extent of each cluster is calculated in order to identify the largest one. Note that, to avoid any size effect, the size of the largest cluster is normalized by that of the simulation box, so that percolation corresponds to a relative size of 1.

Figure 6 shows the evolution of the size of the largest defect cluster as a function of the deposited energy. We observe that the largest cluster size increases gradually upon irradiation. At a critical value of deposited energy, the size of the largest cluster equals that of the simulation box, which denotes the percolation of SRO defects through the atomic network. Note that this behavior is equivalent to the percolation of sites showing a given state (here, defective Si atoms, i.e., with $q_3 < 0.7$) within a three-dimensional (3D) lattice [37,38]. Following percolation theory, the size of the largest defect clusters $L_{\max}$ is then given by

$$L_{\max} = (p_c - p)^{-\nu}, \tag{2}$$

where p is the fraction of defective tetrahedra, p_c is the percolation threshold, and ν is the critical exponent of percolation. Here, we find $p_c = 0.21$ and $\nu = 1.14$. Despite the disordered nature of the atomic network considered herein, we observe that these percolation constants are fairly similar to those obtained in the case of percolation within a 3D

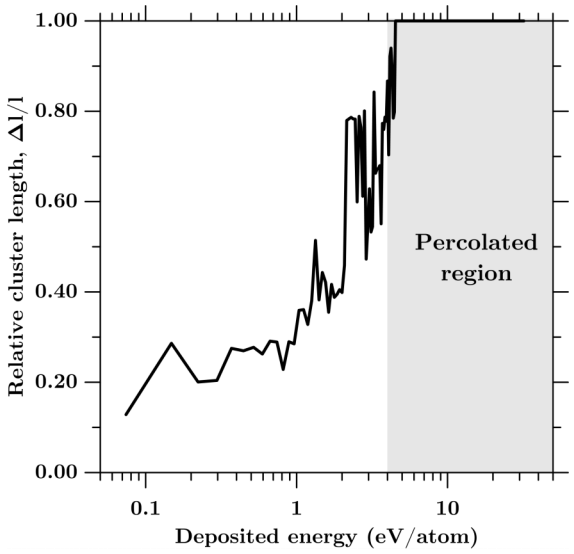

FIG. 6. Maximum spatial extent of short-range-order (SRO) defects clusters, normalized by the size of the simulation box, as a function of the deposited energy. The gray region indicates the domain of deposited energy at which SRO defects percolate, which corresponds to the glassy state (see Fig. 4).

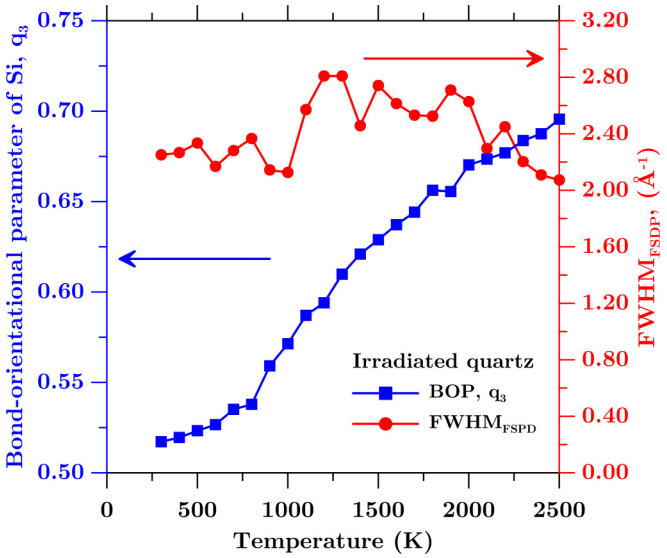

FIG. 7. Evolution of the bond-orientational parameter (BOP) of Si atoms, q_3 (left axis), and FWHM (right axis) of the FSDP of fully irradiated quartz as a function of the annealing temperature.

fcc or bcc lattice [37,38]. Interestingly, we observe that the percolation threshold coincides with the deposited energy at which the amount of SRO defects plateaus and MRO defects start to accumulate (see Fig. 5), that is, it coincides with the amorphous-to-glassy transition. Hence, the present results support our proposed mechanism, that is, that the percolation of SRO defects renders the network macroscopically flexible, which permits the formation of MRO defects and prevents further accumulation of additional energetically unfavorable SRO defects upon further energy deposition.

Finally, we assess the respective roles of the SRO and MRO defects in controlling the response of disordered quartz upon annealing, that is, in determining whether irradiated quartz behaves like an amorphous or glassy material. Toward that end, we track the evolution of q_3 and the FWHM of the FSDP as a function of the annealing temperature. As shown in Fig. 7, we observe that q_3 increases upon annealing, whereas the FWHM of the FSDP remains fairly constant, the coherence length remaining close to 3.2 Å. This demonstrates that, upon annealing, SRO defects can be "healed," whereas MRO defects remain stable. This can be understood as follows. When exposed to annealing, the atoms of the network gain some kinetic energy, which allows them to jump over some energy barriers that could not be overcome at lower temperature. This enables the system to relax toward more stable energy states, that is, the equilibrium crystalline or liquid states. At this stage, most SRO defects can be relaxed since this only requires local reorganizations of the network, that is, such relaxation is associated with rather small energy barriers. In contrast, the relaxation of MRO defects involves large-scale collective reorganizations of atoms, and, hence, it is associated with higher energy barriers, which would require higher temperature (i.e., $>T_m$) to be overcome. As such, at low deposited energy, SRO defects can be relaxed so that the system can reorganize toward its lower state of energy by recrystallizing—thereby acting like amorphous solids. However, at higher deposited energy, the presence of MRO defects kinetically prevents the system from relaxing toward the crystalline state. In this situation, since the crystalline state is not achievable, it becomes more favorable for the system to relax toward a disordered configuration with a well-defined SRO while retaining a disordered MRO, that is, a glassy configuration. In this regime, irradiated quartz then behaves like a glassy solid. The percolation of SRO defects and the appearance of MRO defects, therefore, explain the amorphous-to-glassy transition observed herein.

IV. DISCUSSION

Altogether, these results offer an intuitive atomic basis for the distinction between amorphous and glassy disordered networks. The mechanism proposed herein is consistent with the observation that covalent atomic networks subjected to irradiation tend to evolve toward their glassy counterpart upon the accumulation of defects [39–41]. It is also consistent with the fact that atomic networks primarily comprising ionic bonds feature a high resistance to irradiation [2,40]. Indeed, ionic bonds are largely nondirectional, which facilitates local structural reorganizations after any irradiation damage. This effectively prevents the accumulation of SRO defects. The absence of any percolation of SRO defects prevents the formation of MRO defects, which, in turn, facilitates recrystallization and prevents the network from featuring any irreversible amorphous-to-glassy transition upon irradiation. This idea is consistent with the observation that, besides irradiation, a crystal-to-glass transition can be induced by the accumulation of structural damage caused, e.g., by the introduction of structural frustration [42], insertion of dopants [43–45], or mechanical grinding [46].

More generally, the present results also offer some insights into the long-standing problem of the structural origin of the

propensity for a given disordered atomic network to crystallize [47–49]. It was originally suggested by Zanotto *et al.* that glasses featuring homogeneous nucleation generally present a density that is close to that of the crystal, in contrast to glasses featuring heterogeneous crystallization [50]. This generally supports the idea that a structural dissimilarity between a glass and its isochemical crystal could decrease the propensity for crystallization. However, considering the density alone appears to be too simplistic, as some glasses feature a good resistance to homogeneous crystallization despite showing a density that is comparable to that of their counterpart crystal [51]. Other structural features, such as the spatial distribution of network modifiers [52], coordination numbers [53], or $Q^{(n)}$ units [54], were shown to present only a partial correlation with the propensity for homogeneous crystallization [47,51].

The present results suggest instead a more contrasted picture. (i) An atomic network presenting a SRO that is distinct from that of its corresponding crystal and a MRO that is similar to that of the crystal should feature a high propensity for crystallization. Indeed, SRO defects can easily be relaxed, but they come with a high-energy cost and, as such, their presence acts as a driving force for crystallization. In turn, the absence of MRO defects reduces the extent of kinetic resistance to crystallization. (ii) In contrast, atomic networks presenting a MRO that differs from that of the crystal require some collective atomic rearrangements to crystallize, which results in a strong kinetic resistance to crystallization. In addition, MRO defects come with a low-energy cost and, as such, they do not contribute significantly to increasing the driving force for crystallization.

Therefore, these results suggest that the propensity for crystallization is largely controlled by the degree of similarity between the MRO of the disordered solid and that of the crystal, rather than the overall structural similarity, at all length scales. We expect such concepts to be relevant to understand, predict, and ultimately control the glass-forming ability—or the propensity for crystallization—of liquids cooled under their melting temperature.

V. CONCLUSION

Overall, based on the example of irradiated quartz, this study demonstrates the existence of an amorphous-to-glassy transition in a disordered system. The transition toward a glassy state is shown to arise from the appearance of structural defects within the medium-range order of the atomic network. The formation and accumulation of such medium range is enabled by the percolation of short-range-order defects, which renders the network macroscopically flexible. In turn, as opposed to short-range defects, medium-range defects are not healed upon thermal annealing, which prevents the system from relaxing toward the crystalline state. Therefore, the mismatch between the MRO of the disordered atomic network and that of the crystal controls its propensity to crystallize and, hence, is at the origin of the amorphous-to-glassy transition observed herein.

ACKNOWLEDGMENTS

This research was performed using funding received from the DOE Office of Nuclear Energy's Nuclear Energy University Programs. The authors also acknowledge financial support for this research provided by The Oak Ridge National Laboratory operated for the U.S. Department of Energy by UT-Battelle (LDRD Awards No. 4000132990 and No. 4000143356), National Science Foundation (CMMI: 1235269, CAREER Award No. 1253269), Federal Highway Administration (DTFH61-13-H-00011), and the University of California, Los Angeles (UCLA). Computational resources were provided by the University of California, Los Angeles and San Diego Super Computer Center as part of the HPC@UC program. This manuscript has been coauthored by UT-Battelle, LLC under Contract No. DE-AC05-00OR22725 with the U.S. Department of Energy. The U.S. Government retains, and the publisher, by accepting the article for publication, acknowledges that the U.S. Government retains a nonexclusive, paid-up, irrevocable, worldwide license to publish or reproduce the published form of this manuscript, or allow others to do so, for U.S. Government purposes. The Department of Energy will provide public access to these results of federally sponsored research in accordance with the DOE Public Access Plan (http://energy.gov/downloads/doe-public-access-plan).

[1] A. K. Varshneya, *Fundamentals of Inorganic Glasses* (Elsevier, Amsterdam, 2013).
[2] I. Pignatelli, A. Kumar, K. G. Field, B. Wang, Y. Yu, Y. Le Pape, M. Bauchy, and G. Sant, Sci. Rep. **6**, 20155 (2016).
[3] A. K. Varshneya and J. C. Mauro, Eur. J. Glass Sci. Technol. Part A, Glass Technol. **51**, 28 (2010).
[4] P. K. Gupta, J. Non-Cryst. Solids **195**, 158 (1996).
[5] E. D. Zanotto and J. C. Mauro, J. Non-Cryst. Solids **471**, 490 (2017).
[6] S. K. Deb, M. Wilding, M. Somayazulu, and P. F. McMillan, Nature (London) **414**, 528 (2001).
[7] B. Wang, Y. Yu, I. Pignatelli, G. Sant, and M. Bauchy, J. Chem. Phys. **143**, 024505 (2015).
[8] R. Devanathan, Ph.D. thesis, Northwest University, 1993.
[9] W. J. Weber, J. Mater. Res. **5**, 2687 (1990).
[10] S. Plimpton, J. Comput. Phys. **117**, 1 (1995).
[11] W. G. Hoover, Phys. Rev. A **31**, 1695 (1985).
[12] A. H. Mir, M. Toulemonde, C. Jegou, S. Miro, Y. Serruys, S. Bouffard, and S. Peuget, Sci. Rep. **6**, 30191 (2016).
[13] A. C. Van Duin, S. Dasgupta, F. Lorant, and W. A. Goddard, J. Phys. Chem. A **105**, 9396 (2001).
[14] H. Manzano, S. Moeini, F. Marinelli, A. C. T. van Duin, F.-J. Ulm, and R. J.-M. Pellenq, J. Am. Chem. Soc. **134**, 2208 (2012).
[15] Y. Yu, B. Wang, M. Wang, G. Sant, and M. Bauchy, J. Non Cryst. Solids **443**, 148 (2016).
[16] F. A. Lindemann, Phys. Z. (West Germany) **11**, 609 (1910).

[17] J. M. Lane, Phys. Rev. E **92**, 012320 (2015).
[18] K. Vollmayr, W. Kob, and K. Binder, Phys. Rev. B **54**, 15808 (1996).
[19] M. Parrinello and A. Rahman, J. Appl. Phys. **52**, 7182 (1981).
[20] P. J. Steinhardt, D. R. Nelson, and M. Ronchetti, Phys. Rev. B **28**, 784 (1983).
[21] M. Bauchy, J. Chem. Phys. **141**, 024507 (2014).
[22] N. A. Krishnan, B. Wang, Y. Le Pape, G. Sant, and M. Bauchy, J. Chem. Phys. **146**, 204502 (2017).
[23] N. P. Bansal and R. H. Doremus, *Handbook of Glass Properties* (Elsevier, Amsterdam, 2013).
[24] B. Wang, N. A. Krishnan, Y. Yu, M. Wang, Y. Le Pape, G. Sant, and M. Bauchy, J. Non-Cryst. Solids **463**, 25 (2017).
[25] W. H. Zachariasen, J. Am. Chem. Soc. **54**, 3841 (1932).
[26] L. W. Hobbs, C. E. Jesurum, V. Pulim, and B. Berger, Mater. Sci. Eng. A **253**, 16 (1998).
[27] C. E. Jesurum, V. Pulim, and L. W. Hobbs, J. Nucl. Mater. **253**, 87 (1998).
[28] R. Devanathan, J. N. Mitchell, K. E. Sickafus, W. J. Weber, and M. Nastasi, Mater. Sci. Eng. A **253**, 131 (1998).
[29] R. Devanathan, W. J. Weber, J. N. Mitchell, K. E. Sickafus, and M. Nastasi, *Radiation Response of Rhombohedral Oxides* (Los Alamos National Lab., Los Alamos, NM, 1997).
[30] L. W. Hobbs, *Radiation-Induced Topological Disorder in Irradiated Network Structures* (MIT Press, Cambridge, MA, 2002).
[31] W. Primak, Phys. Rev. **110**, 1240 (1958).
[32] S. R. Elliott, Phys. Rev. Lett. **67**, 711 (1991).
[33] M. Micoulaut and M. Bauchy, Phys. Status Solidi B **250**, 976 (2013).
[34] S. R. Elliott, Nature (London) **354**, 445 (1991).
[35] P. Scherrer, in *Kolloidchemie Ein Lehrbuch* (Springer, Berlin Heidelberg, 1912), pp. 387–409.
[36] N. M. A. Krishnan, B. Wang, Y. Yu, Y. Le Pape, G. Sant, and M. Bauchy, Phys. Rev. X **7**, 031019 (2017).
[37] C. D. Lorenz and R. M. Ziff, J. Phys. Math. Gen. **31**, 8147 (1998).
[38] J. Wang, Z. Zhou, W. Zhang, T. M. Garoni, and Y. Deng, Phys. Rev. E **87**, 052107 (2013).
[39] J. F. Denatale and D. G. Howitt, Nucl. Instrum. Methods Phys. Res. Sect. B **1**, 489 (1984).
[40] K. Trachenko, J. Phys.: Condens. Matter **16**, R1491 (2004).
[41] S. X. Wang, L. M. Wang, R. C. Ewing, and R. H. Doremus, J. Non-Cryst. Solids **238**, 198 (1998).
[42] P. Yunker, Z. Zhang, and A. G. Yodh, Phys. Rev. Lett. **104**, 015701 (2010).
[43] S. J. Gerbode, D. C. Ong, C. M. Liddell, and I. Cohen, Phys. Rev. E **82**, 041404 (2010).
[44] R. Higler, J. Appel, and J. Sprakel, Soft Matter **9**, 5372 (2013).
[45] M. Li and W. L. Johnson, Phys. Rev. Lett. **70**, 1120 (1993).
[46] P. Mura, M. Cirri, M. T. Faucci, J. M. Ginès-Dorado, and G. P. Bettinetti, J. Pharm. Biomed. Anal. **30**, 227 (2002).
[47] E. D. Zanotto, J. E. Tsuchida, J. F. Schneider, and H. Eckert, Int. Mater. Rev. **60**, 376 (2015).
[48] V. M. Fokin, E. D. Zanotto, N. S. Yuritsyn, and J. W. P. Schmelzer, J. Non-Cryst. Solids **352**, 2681 (2006).
[49] J. C. Mauro, C. S. Philip, D. J. Vaughn, and M. S. Pambianchi, Int. J. Appl. Glass Sci. **5**, 2 (2014).
[50] E. D. Zanotto and E. Müller, J. Non-Cryst. Solids **130**, 220 (1991).
[51] E. D. Zanotto, Int. J. Appl. Glass Sci. **4**, 105 (2013).
[52] E. Müller, K. Heide, and E. D. Zanotto, Z. Krist.-Cryst. Mater. **200**, 287 (2010).
[53] E. Muller, K. Heide, and E. D. Zanotto, J. Non-Cryst. Solids **155**, 56 (1993).
[54] J. Schneider, V. R. Mastelaro, H. Panepucci, and E. D. Zanotto, J. Non-Cryst. Solids **273**, 8 (2000).